Supplementary Figures

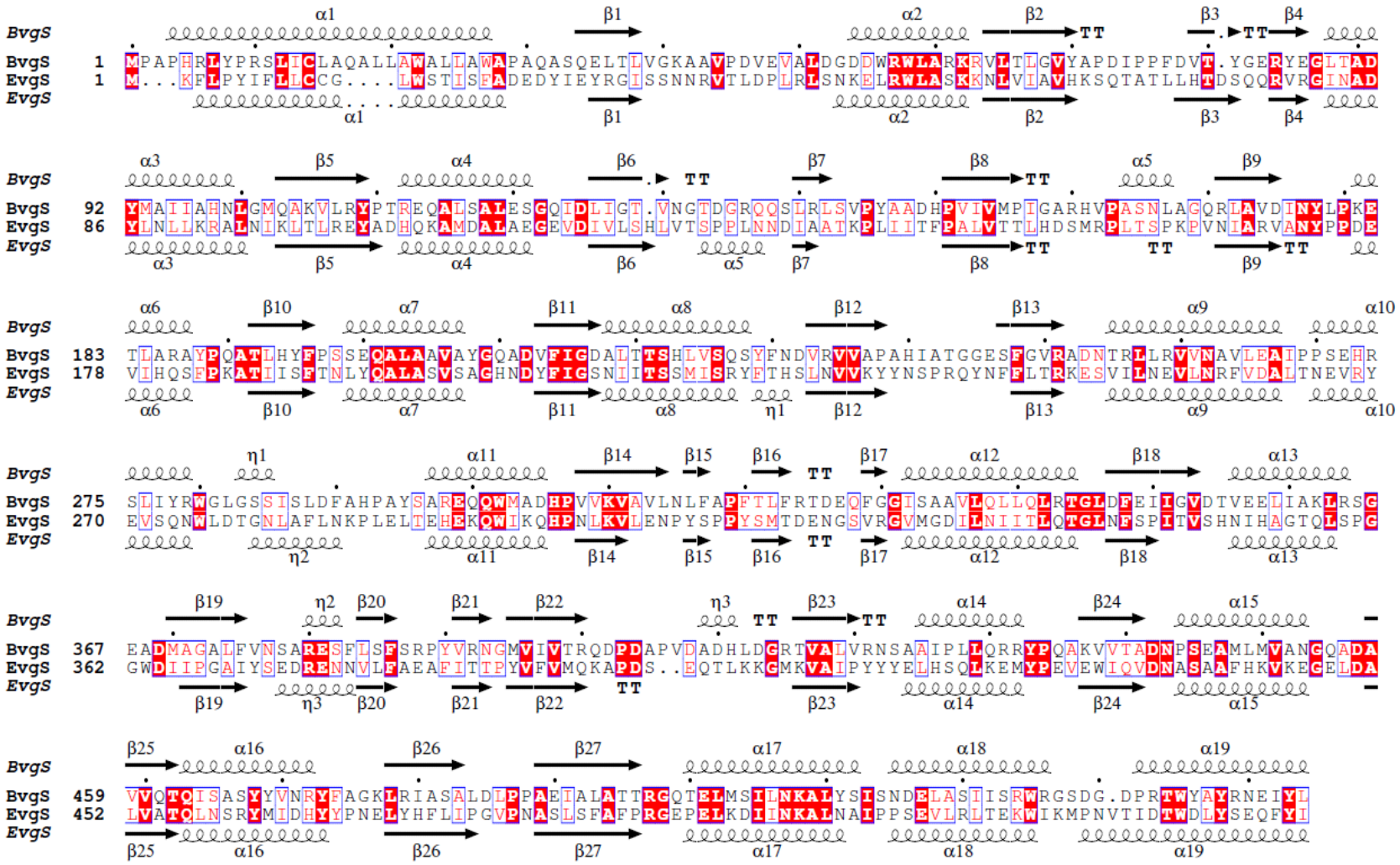

Figure S1: Structural alignment of BvgS and EvgS periplasmic regions (figure prepared using Espript 3 based on the MAFFT–generated sequence alignment). The secondary elements above the alignment correspond to the experimental structure of the periplasmic domain of the BvgS (4Q0C.pdb), although the numbering of the alpha-helices is slightly different to that used in Dupré *et al*., 2015 as directly extracted from the PDB file. The secondary structure elements shown for EvgS are based on the model presented in this paper. Numbering for each protein runs from the initiator methionine (thus including the signal sequence) to the edge of the available structural data on the periplasmic domains.

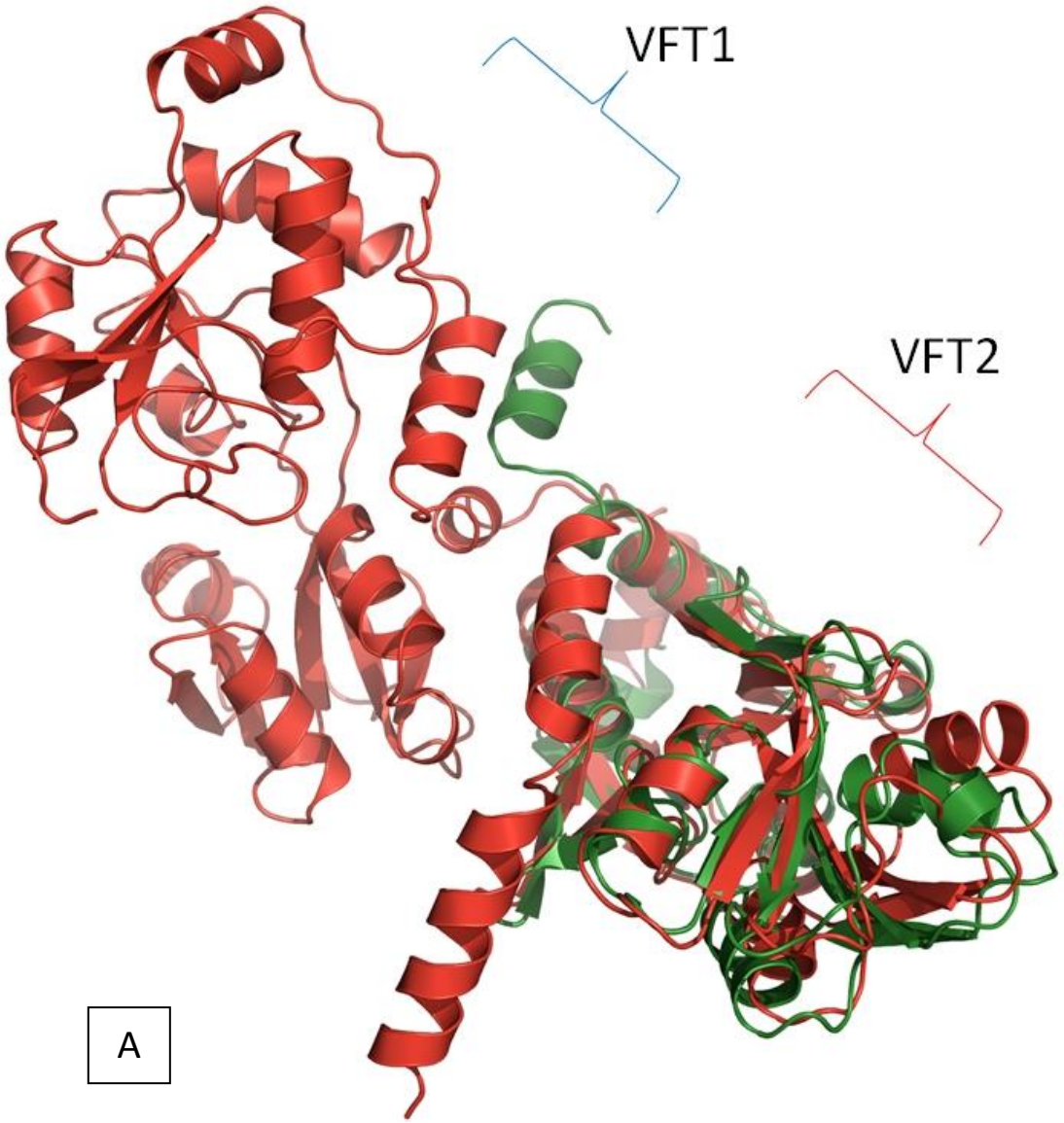
VFT1
VFT2
A

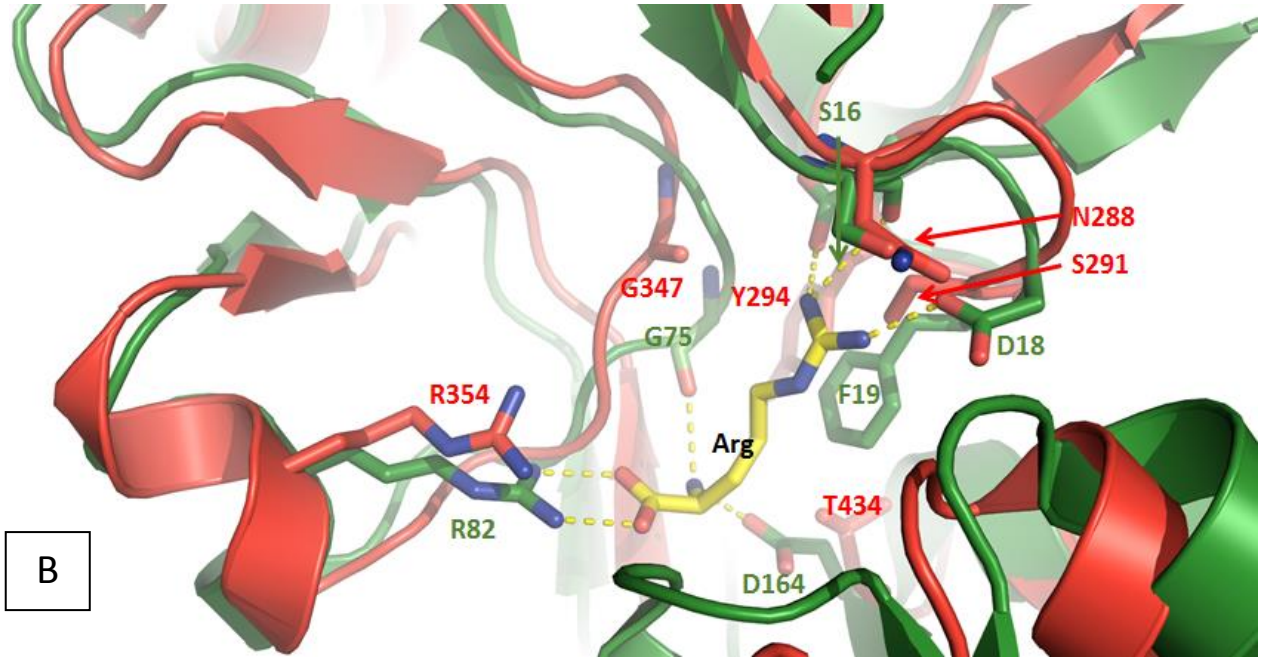

Figure S2: The VFT2 domain of EvgS shows high homology to periplasmic amino-acid binding proteins and may be involved in ligand binding.

A) A superposition of VFT2 domain of the modelled EvgS with the ArgBP from *Thermatoga maritima* (4PSH.pdb) shows a close structural relationship. The VFT2 of EvgS model (and BvgS) respectively superpose with an rmsd of approx. 2.4 Å over the C-alpha backbone of the ArgBP.

B) A close-up of the Arg coordination in the ArgBP (green) and corresponding region of the EvgS, showing the conserved Arg residue involved in the coordination of carboxyl-groups of the amino-acid ligands. R82 in ArgBP in EvgS corresponds to R354 in ArgBP. Its position is retained in the model making it plausible that it may coordinate a carboxylate-containing ligand. Additional residues are shown that are either equivalent or provide a similar binding environment – e.g. F19 in ArgBP is involved in cation-pi interaction with the guanidinium group of the arginine, and while there is no direct equivalent on the same position in the corresponding loop in EvgS, the location of Y294 may allow it to contribute to binding of a similar ligand, while G75 that coordinates the alpha-amino group of the Arg in ArgBP has a direct equivalent in G347 in EvgS. Note that the overlay shown in Figure S2B represents an unliganded form of the EvgS, while the crystal structure of the ArgBP is a more tight, liganded form; binding of a potential ligand to EvgS may change the conformation of the pocket. The pocket as presented in EvgS has no obvious steric clashes with a potential ligand, and furthermore critical coordinating residues are conserved as shown, so it may serve as a site of binding for a as yet unidentified, carboxylate group containing ligand.

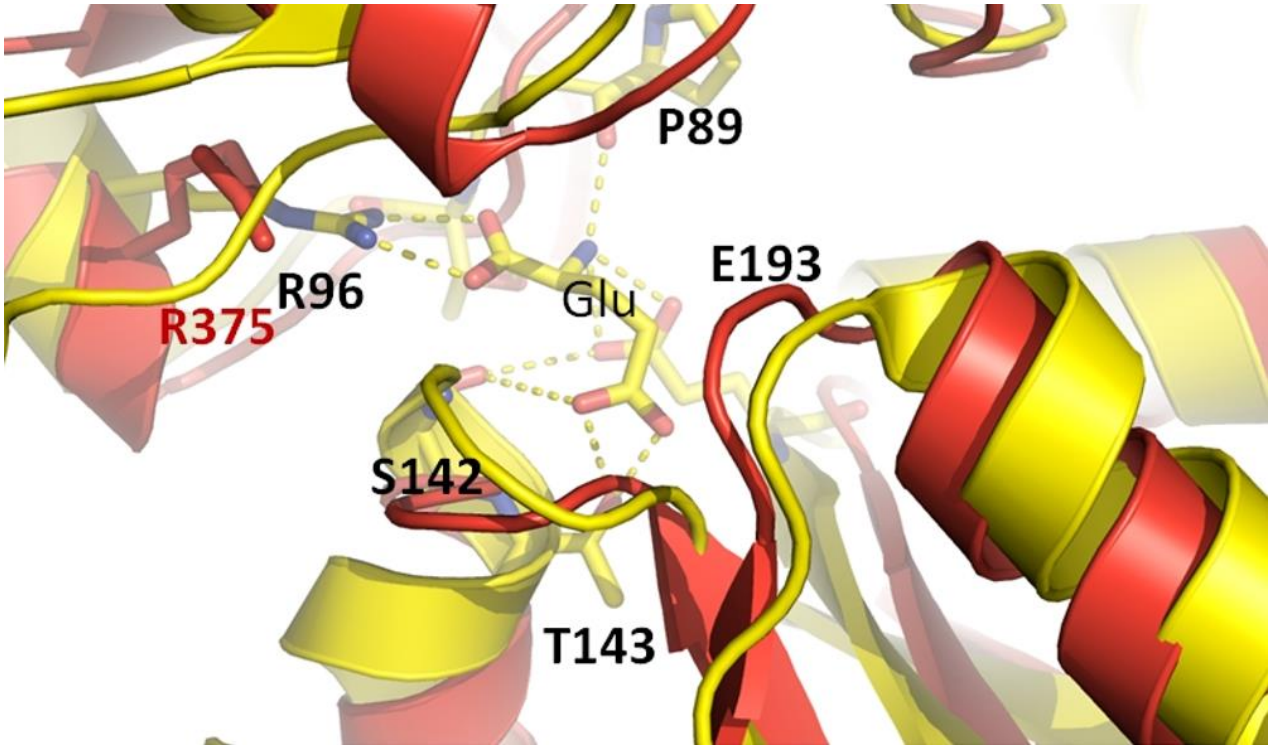

Figure S3. Cutaway view of the VFT2 domain potential ligand-binding region of the modelled EvgS (red) overlayed with the GluA2 (3SLS, yellow) showing the coordination of the amino-acid ligands by conserved Arg-residue (R96 in GluA2, corresponding to Arg375 in EvgS). Other important residues involved in Glu coordination are highlighted.

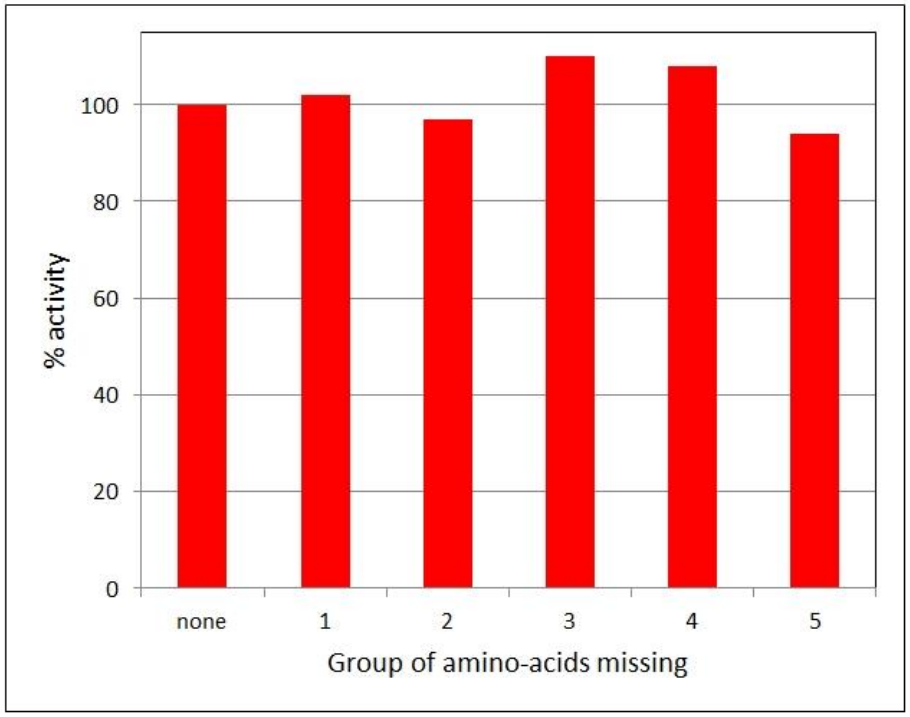

Figure S4: % EvgS-induced activity of *ydeP-lacZ* fusion at pH 5.6 when different groups of amino-acids omitted from growth medium. Groups are 1: N, Q, D, E; 2: K, R, H; 3: W, Y, F; 4: G, L, V, A, I, M; 5: S, C, P.

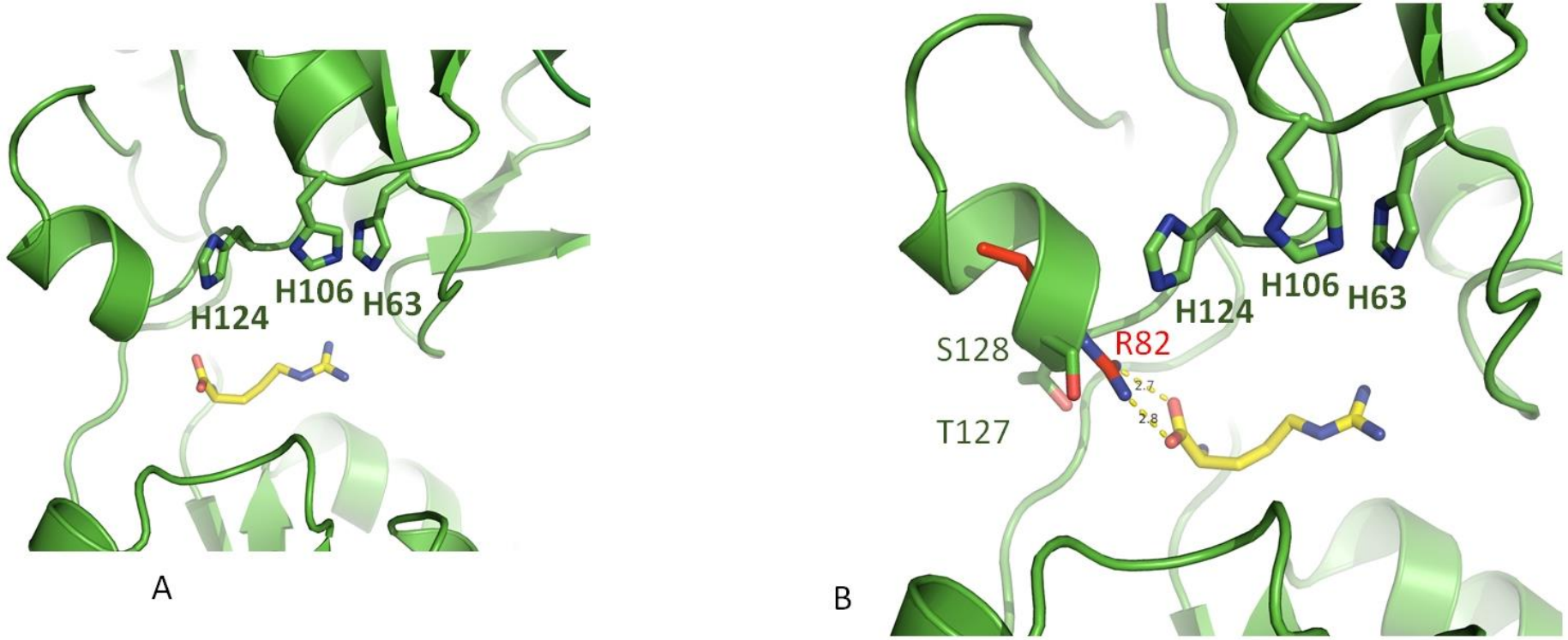

Figure S5: VFT1 of EvgS presents a peculiar His-cluster in proximity to the ligand binding pocket.

Note that the VFT1 is modelled in an open conformation, which would not occur if a ligand were bound.

A) A close-up of the VFT1 domain cleft with 3 His-residues possibly protruding into the ligand binding cavity. The position of the Arg moiety is shown based on the superposition of the ArgBP from *T.maritima* (PSH.pdb) over VFT1 domain. (Note that the overlay produces an RMSD of over 4 Å as compared with 2.3 Å for VFT2 domain and as such is less reliable).

B) Same, with additional residues showing the relative position of the R82 (in red sticks representation, numbered as in the PDB file) involved in Arg coordination in ArgBP, and the lack of conservation in the corresponding region of EvgS, residues T127 and S128 occupying the orthologous position in EvgS.

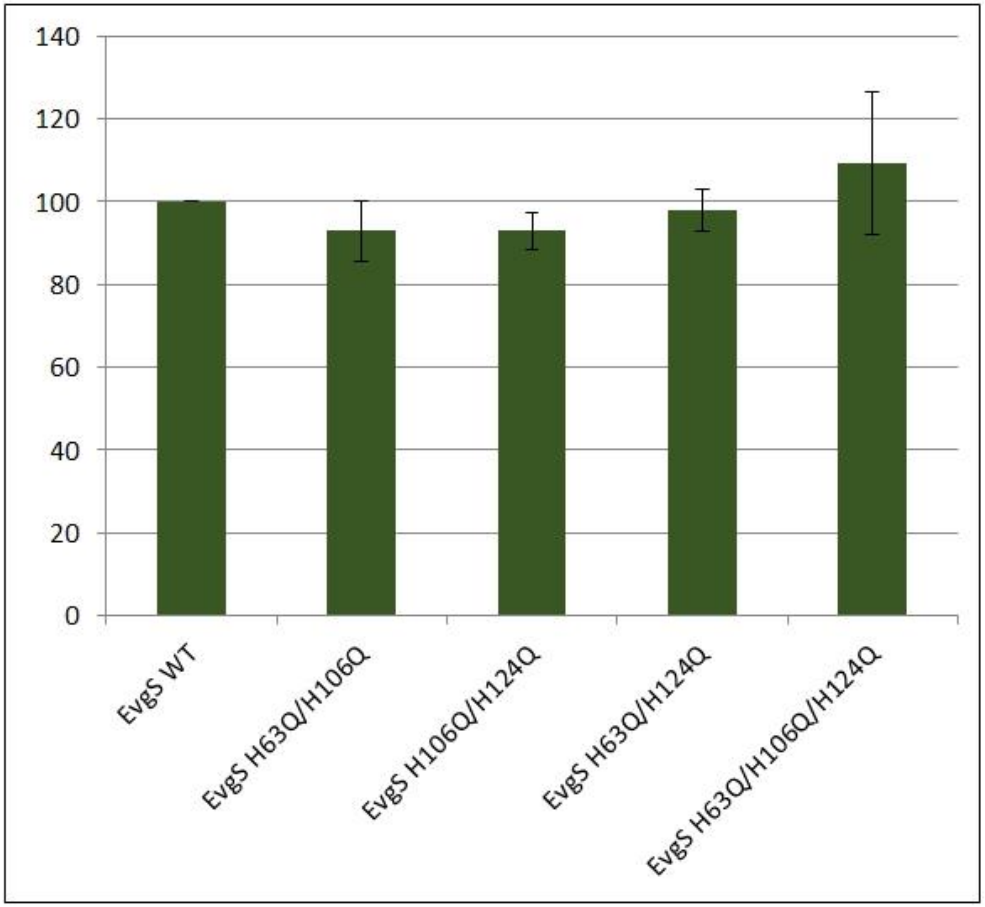

Figure S6: Relative % induction at pH 5.6 of all possible pairwise and triple combinations of EvgS H63Q, H106Q, and H124Q, with wild-type (wt) shown for comparison.

Supplementary Table S1: Bacterial strains and plasmids

Strains	Features	Source
BL21(DE3*)	Host for protein expression	1
HSTO8	Super-competent strain for high-efficiency transformations	Takara-Bio
MG1655	wild type *E. coli* K12	2
MG1655 Δ*evgS*::*cat ydeP-lacZ kan*^{R}	strain with chromosomal evgS inactivated with a chlormaphenicol marker and harbouring the promoter probe fusion, linked to a *kan*^{R} gene	3
Plasmids:		
pBAD24-his	vector backbone for cloning with 6X-his tag	Invitrogen

pBADEvgS	Gene for evgS cloned into pBAD-TOPO	3
pBADEvgS-Cyt	Cytoplasmic domains of *evgS* cloned into pBAD24-his	This work
PBADEvgS-Cyt S600I	cytoplasmic domain of evgS harbouring the S600I mutation cloned into pBAD24	This work
pET41c+	Vector backbone for cloning cytoplasmic domain of EvgS	Lucigene

References in Supplementary Table S1.

1. Studier FW, Moffatt BA. 1986. Use of bacteriophage T7 RNA polymerase to direct selective high-level expression of cloned genes. J Mol Biol. 189: 113-130.
2. Blattner FR, Plunkett G 3rd, Bloch CA, Perna NT, Burland V, Riley M, Collado-Vides J, Glasner JD, Rode CK, Mayhew GF, Gregor J, Davis NW, Kirkpatrick HA, Goeden MA, Rose DJ, Mau B, Shao Y. 1997. The complete genome sequence of Escherichia coli K-12. Science 277: 1453-1462.
3. Eguchi Y, Utsumi R. 2014. Alkali metals in addition to acidic pH activate the EvgS histidine kinase sensor in Escherichia coli. J Bacteriol 196: 3140-3149.